Selenium/Zeolite Y Nanocomposites

ANDREAS GOLDBACH* AND
MARIE-LOUISE SABOUNGI
Centre de Recherche sur la Matière Divisée, Orléans, France

Received November 30, 2004

ABSTRACT
Confinement in molecular sieves is a promising strategy for fabricating nanostructured semiconductor assemblies with a highly uniform size and shape distribution. However, disorder effects often hamper the engineering of matrix-embedded cluster materials with specific properties. The host−guest interaction is a key factor for optimizing their structure, electronic characteristics, and stability. In this Account, we describe how the interplay between confined selenium and extraframework cations in zeolite hosts can be used to tailor these properties and to produce well-defined semiconductor nanocomposites with band gaps in the visible range.

Introduction

Selenium is an important photoconductor used in rectifiers, photocopiers, photographic exposure meters, and solar cells.[1] It has many favorable properties including low glass transition temperature (30 °C), low melting point (217 °C), and high photoconductivity (ca. 8×10^4 S/cm), and it can be converted into other functional semiconductors with interesting optical (e.g., CdSe)[2] and magnetotransport (e.g., Ag_2Se)[3] properties. Therefore, selenium nanomaterials have received considerable attention.[4−8] Selenium exhibits a remarkable structural diversity[1] in the bulk with trigonal (*t*-Se, helical chains), monoclinic (*m*-Se, Se_8 rings), rhombohedral (*r*-Se, Se_6 rings), and amorphous forms (*a*-Se, disordered chains),[9] making it an ideal subject for investigating the effect of confinement on a semiconductor. In the vicinity of the narrowest electronic gap, the band structures of *t*-Se and *a*-Se are determined by the exchange of electron density between nonbonding valence and antibonding conduction bands of neighboring chains.[9] These interchain correlations are reduced in disordered *a*-Se relative to crystalline *t*-Se and decline further in Se nanocrystals. Thus, nanostructured and molecular Se assemblies exhibit altered optoelectronic properties that could have considerable potential for applications in solar energy conversion, photocatalysis, photoluminescent sensors, and nonlinear optics if sufficiently uniform and stable nanomaterials were produced. We show that both objectives can be achieved by embedding Se into inert nanoporous matrices such as zeolites.

Zeolites are three-dimensional crystalline networks of edge-linked, oxygen-sharing AlO_4^- and SiO_4 tetrahedra that contain 5−13 Å wide pore systems.[10] Mobile and readily exchangeable extraframework cations neutralize the negative framework charges due to the AlO_4^- units. The regular dimensions of channels and voids make it possible to implement well-defined nanowires and cluster assemblies with narrow size distributions.[11,12] Furthermore, zeolites are insulators with band gaps around 5 eV, making them excellent supports for optically active host−guest materials.[13] The more than 60 topologically distinct framework types offer a large variety of one-, two-, and three-dimensional pore systems.

Selenium/zeolite composites were first described by Bogomolov and co-workers[14−16] and subsequently became subjects of intense study.[17−24] The majority of work used sodium zeolites with archetypical pore systems containing 6−7 Å wide one-dimensional channels (cancrinite, mordenite) or three-dimensionally interconnected 11−13 Å wide cages with 4−7.5 Å wide entrances (zeolite 4A, zeolite X). The confinement of Se in electroneutral molecular sieves such as AFI (aluminophosphate with 7.3 Å channels) and decadodecasil 3R (SiO_2 framework with ellipsoidal cages of 9.2 Å maximum diameter) was investigated more recently.[18,25−27] Lately, computational studies have also been carried out on such composites.[28,29] Wide-pore systems often accommodate multiple Se species (e.g., AFI hosts Se_8 and regular chains[26] and zeolite Y hosts Se_8 and disordered chains[30]). The formation of single Se entities is favored in matrices with narrow pores and isolated cages (e.g., Se_6 rings in decadodecasil 3R,[27] Se_{12} rings in zeolite 4A,[21] and Se_2^{2-} dianions in cancrinite[23]).

While the structural and electronic properties of Se confined in zeolites have been widely explored, little attention has been paid to the host−guest interaction. In particular, the extraframework cations are propitious interaction sites for the electron-rich chalcogens. The resulting electronic correlations have a profound impact on the behavior of the confined Se. However, zeolites containing cations other than Na^+ have been rarely used for the confinement of Se,[19,20] and there have been no systematic studies on the effects exerted by metal ions on Se. We therefore embarked on an investigation of the role played by extraframework cations in the structural organization of confined Se[30−33] and how they affect the electronic properties[33−35] and the thermodynamic and

Andreas Goldbach was born in Germany and obtained his Ph.D. in Chemistry at the University of Marburg in 1993. After periods at Marburg, Argonne National Laboratory (USA), the University of Birmingham (UK), and the Fraunhofer Institute for Interfacial Engineering and Biotechnology at Stuttgart, he presently is a visiting scientist at the Centre de Recherche sur la Matière Divisée in Orléans, France. His research interests include the interdependence of structure, electronic properties, and reactivity of mesoscopic semiconductors and metals and transport phenomena in nanoporous materials and inorganic membranes.

Marie-Louise Saboungi was born in Lebanon and received her Ph.D. in 1973 from the University of Aix-Marseille, France. She then joined the Argonne National Laboratory where she subsequently became a senior scientist. Her research at ANL was dedicated to establishing relationships between the microscopic structure and dynamics of different kinds of disordered condensed matter—including liquids, glass, and crystalline materials with translational or orientational disorder—and their macroscopic thermodynamic and transport properties. She and her collaborators extended this approach to nanocrystalline and clustered materials and to polymer electrolytes in both bulk and nanocomposite forms. Three years ago, Dr. Saboungi was appointed Professor of Physics at the University of Orleans and Head of the CNRS Center for Research on Divided Matter in Orleans, France. She is a Fellow of the American Physical Society and the American Association for the Advancement of Science.

10.1021/ar040282y CCC: $30.25
Published on Web 07/06/2005

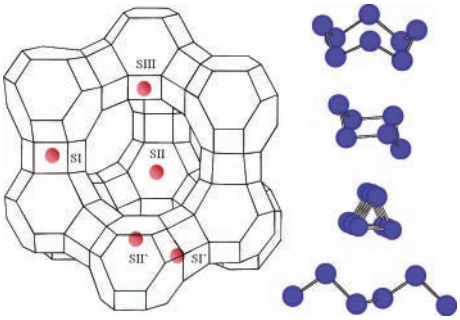

FIGURE 1. Faujasite supercage with location of cation sites and scaled Se_8 (D_{4d}) and Se_6 (D_{3d}) rings and helical chains viewed along and parallel to the *c*-axis.

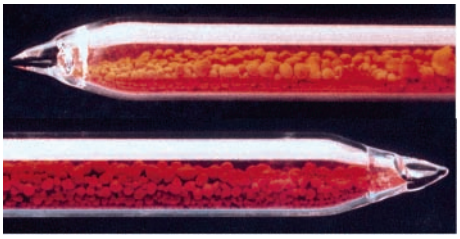

FIGURE 2. Ca−Y (top) and La−Y (bottom) zeolite holding ca. 12 Se atoms per supercage.

optical stability of the nanocomposites.[36−39] Zeolite Y was chosen as host because the faujasite framework provides the largest pores among natural aluminosilicates, and the number of cations accessible to the incorporated Se can be readily reduced, even to zero if desired.

Composites. The zeolite Y unit cell ($M_{57/x}^{x+}(AlO_2^-)_{57}(SiO_2)_{135}$) includes eight 13 Å wide supercages (Figure 1) interconnected through four 7.5 Å wide windows.[10] These cages result from the tetrahedral junction of 6.5 Å wide sodalite cages through hexagonal prisms. The extraframework M^{x+} cations prefer sites inside the prisms (SI) and sodalite cages (SI′, SII′). In the supercages, the sites above the 2.4 Å wide sodalite cage apertures (SII) are favored over those within the large windows (SIII). The cation arrangement depends on their type and number: SII positions are occupied in zeolites with monovalent or divalent cations, while SIII sites are only taken in alkali-exchanged zeolites. Polyvalent rare earth metal ions form oxygen-bridged clusters within the sodalite cages. Liquid or gaseous Se is readily incorporated into the supercages, but the sodalite cage apertures are too narrow to admit even dimers. For comparison, we show scaled structural units of crystalline Se allotropes in Figure 1: the Se_8 ring (approximate covalent diameter 7.5 Å), Se_6 ring (6.6 Å), and Se helix (4.5 Å).

Sorption of Se into dehydrated Y zeolites yields yellow to burgundy powders, the tinge depending on Se concentration and M^{x+} ions (Figure 2). Up to 13 Se atoms per supercage (15 at. % Se) can be encapsulated at 350 °C (≅10 Torr Se vapor pressure), based on the residue-free uptake of weighed Se amounts by the chemically analyzed zeolites.[30,33,39] We typically studied composites with 10−12 Se atoms per supercage. Transmission electron micrographs showed no external Se particles.[31] Bogomolov and co-workers were able to incorporate ca. 20 Se atoms into the isostructural zeolite Na-X using molten Se at elevated pressures.[16] This still corresponds to only 50% of the theoretical maximum capacity based on the supercage diameter (13 Å) and the density of *t*-Se (4.8 g/ cm^3).

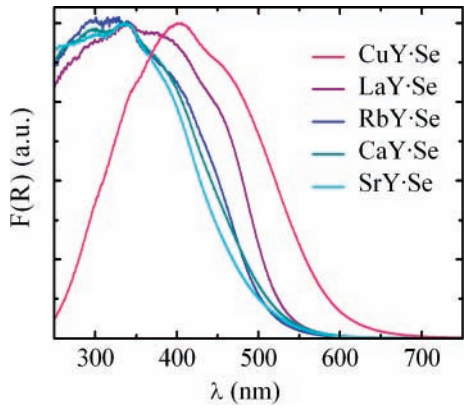

FIGURE 3. Optical spectra of Se confined in various cation-exchanged Y zeolites.

Table 1. Band Gaps of *a*-Se, *t*-Se, and *m*-Se and of Se Confined in Various Cation-Exchanged Y Zeolites[33,34,39]

	bulk Se modifications			Se in M−Y zeolites (M = cation)				
Se form	*a*-Se	*t*-Se	*m*-Se	Rb^+	Sr^{2+}	Ca^{2+}	La^{3+}	Cu^{2+}
indirect gap (eV)	2.05				2.45	2.38	2.35	2.09
direct gap (eV)		1.95	2.53	2.62	2.77	2.72	2.47	

Optical Spectra. Figure 3 displays UV/vis spectra of Se confined in different cation-exchanged Y zeolites, derived via the Kubelka−Munk formalism from diffuse reflectance measurements of the composites relative to empty zeolites.[30,33,34,39] The spectra are very similar for Se confined in the alkali and alkaline earth-exchanged zeolites Rb−Y, Ca−Y, and Sr−Y. In the La−Y composite, the optical density is higher at low energies, and in Cu−Y, the whole Se absorption spectrum is red-shifted. Bulk Se forms exhibit direct (*m*-Se) and indirect (*a*-Se) band gaps, as derived from the energy dependence of the absorption coefficient α at the onset of absorption.[9] We used the same procedures to assess the band gaps of the confined Se since the composites contain Se_8 rings and disordered chains such as those bulk allotropes (vide infra).[30,33,34,39] Most composite Se band gaps are considerably larger than those of the bulk selenium forms (Table 1).[33,34,39] The blue shift of the Se absorption edge results from the loss of intermolecular Se−Se interactions. The transfer of electron density from nonbonding lone-pair to antibonding π^* orbitals narrows the band gap, especially in *t*-Se and *a*-Se,[9] but within the zeolite pores, this electron density exchange is substantially reduced due to the separation of Se chains and rings; thus, the gap between valence and conduction band opens up.[34,35] In zeolite Cu−Y, this effect is compensated through electronic interactions between the Cu^{2+} and Se: Cu-3d and Se lone-pair states presumably form bonding and antibonding hybrid states within the Se band gap, reducing it to a value similar to that of *a*-Se.[33] This interaction with extraframework transition metal ions

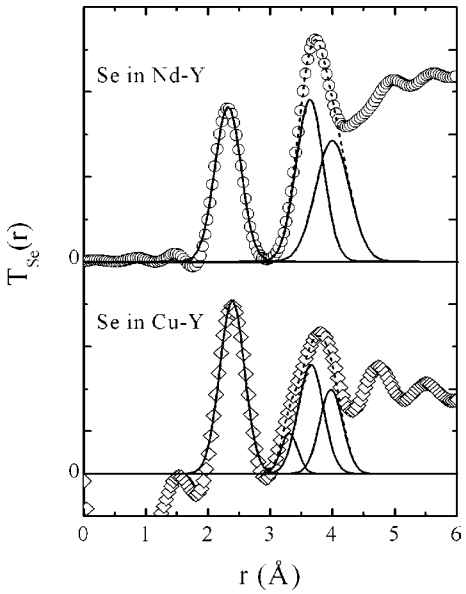

FIGURE 4. Difference pair distribution functions of Se confined in Nd−Y and Cu−Y.

opens up the possibility of tailoring the band gap of confined Se. However, the adjustment of electronic properties requires knowledge of the structure of the Se and its interaction with the zeolite counterions.

Short-Range Order. Since the confined Se is not in registry with the faujasite framework, traditional crystallographic techniques cannot be used to determine the chalcogen structure. We therefore carried out anomalous X-ray scattering (AXS) experiments[40,41] to extract Se-specific structural information. A difference structure factor $S_{Se}(Q)$ associated with Se is derived from the difference of two diffraction measurements performed at incident energies of ca. 20 and a few hundred eV below the Se K-absorption edge, where the atomic scattering factor of Se changes rapidly while those of other elements in the material remain essentially constant.[40,41] Fourier transformation of $S_{Se}(Q)$ yields a difference pair distribution function $T_{Se}(r)$ that gives information about the average spatial environment of the Se atoms. This includes Se−Se, Se−O, Se−T (T = Al, Si), and Se−cation correlations, with the first three having an approximately equal weighting around 30%.[33]

Figure 4 shows $T_{Se}(r)$ for Se in Nd^{3+}- and Cu^{2+}-exchanged zeolite Y.[32,33] The broad peaks indicate a considerable variation of bond distances and angles similar to those found in bulk disordered materials. The structural parameters of the Se were determined by fitting Gaussian functions to the first two peaks.[32,33] The first peak can be represented by a single Gaussian and corresponds to the intramolecular Se bonding. The second peak includes unresolved intra- and intermolecular second-neighbor Se−Se and different types of Se−host correlations, requiring at least two Gaussians. Bond distances R, bond angles ϕ, and coordination numbers C obtained from the fit for Se in zeolite Nd−Y are compared to values of bulk Se forms in Table 2.[32] The shortened first-neighbor Se−Se distance $R_1 = 2.32$ Å indicates a strengthening of

Table 2. Short-Range Structural Parameters for Se in Zeolite Nd−Y, La−Y, Ca−Y, and Cu−Y and in Bulk Forms (After Refs 32, 33, and 38)

form		C_1 (Se,Se)	R_1 (Å)	C_2 (Se,Se)	R_2 (Å)	ϕ (deg)
Nd−Y·Se		2.0 ± 0.3	2.32 ± 0.02	4 ± 1	3.66 ± 0.02	104 ± 2
La−Y·Se		2.2 ± 0.3	2.34 ± 0.02	2 ± 1	3.70 ± 0.02	104 ± 2
Ca−Y·Se		2.2 ± 0.3	2.34 ± 0.02	2 ± 1	3.70 ± 0.02	104 ± 2
Cu−Y·Se		(2)	2.39 ± 0.02	(2)	3.65 ± 0.1	100 ± 3
t-Se:	intra	2.0	2.373	2.0	3.716	103.1
	inter			4.0	3.436	
m-Se:	intra	2.0	2.336	2.0	3.72	105.7
	inter			2.9	3.80	
r-Se:	intra	2.0	2.356	2.0	3.64	101.1
	inter			4.0	3.54	
a-Se		2.0	2.36	7 ± 1	3.74	104.8

the intramolecular bonds in confined Se, and the associated coordination number $C_1 = 2$ implies either rings or very long chains. The second peak in $T_{Se}(r)$ for the Nd−Y composite can be fitted by two Gaussian functions centered at 3.66 and 4.00 Å, attributed to Se−Se and Se−framework interactions, respectively. The Se−Se correlation length $R_2 = 3.66$ Å is similar to intramolecular second-neighbor Se−Se distances in *t*-Se and *a*-Se, but the associated coordination number C_2 is much smaller than in the bulk, confirming reduced intermolecular Se−Se interactions. The structural parameters obtained for Se confined in La−Y and Ca−Y zeolites agree within the error limits except that the second-neighbor Se−Se coordination number C_2 is closer to 2, pointing to isolated Se rings or chains.[38] These results imply that intermolecular interactions weaken the intramolecular bonding in bulk *t*-Se and *a*-Se (Table 2).

Evidence for Se−host correlations around 4.0 Å was found in all studied Se/zeolite Y composites,[32,33,38] suggesting that these involve the framework atoms (O, Al, Si) since the interaction of Se with extraframework cations is bound to vary with their number and nature. Indeed, the fit of the second peak in $T_{Se}(r)$ for the Cu−Y composite requires a third Gaussian centered at 3.30 Å in addition to the usual ones at 3.65 and 3.95 Å (Figure 4).[33] This short correlation length can be attributed to strong Cu^{2+}−Se interactions. It is not possible to extract reliable Cu^{2+}−Se coordination numbers because of the low weighting of these correlations (<10%) in $T_{Se}(r)$ and the large uncertainty associated with the 3-Gaussian fit. The long first-neighbor Se−Se distance of 2.39 Å indicates weakened intramolecular Se bonds in Cu−Y due to the strong Cu^{2+}−Se interactions.[33] It also suggests that antibonding hybrid states resulting from the electronic coupling between Cu-d and Se lone-pair states are largely centered on the Se.[33] The interactions between Se and main-group metal ions are much weaker but not negligible, as will be shown next.

Molecular Structure. AXS does not reveal the molecular character of the confined Se. For that, Raman spectroscopy is very efficient since it is more sensitive to Se than to the aluminosilicate framework due to the larger polarizability of the chalcogen. In fact, Se bands dominate the spectra, while zeolite bands appear only under exceptional circumstances.[39] Figure 5 displays Raman spec-

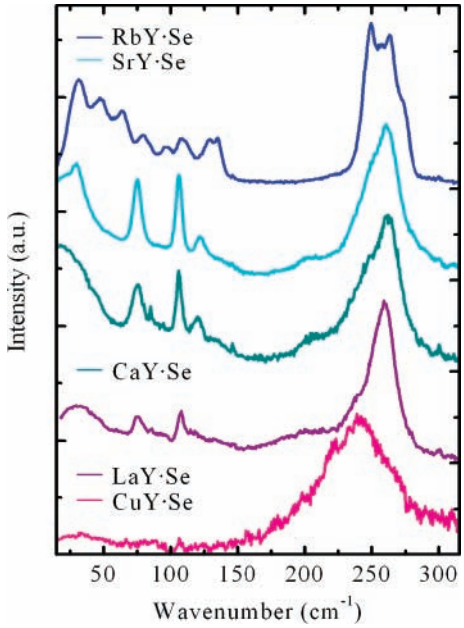

FIGURE 5. Raman spectra of Se confined in various cation-exchanged Y zeolites.

Table 3. Calculated Raman Modes of Se_8 (D_{4d})[44] and Raman Bands of Se_8 Confined in Rb−Y and Sr−Y[30,39] and of Se_8 in *m*-Se[46a]

mode symmetry	E_2	E_2	A_1	E_3	A_1	E_2	E_3	ref
calculated Se_8 (D_{4d})	32	77	106	116	259	274	276	44
Se_8 in Rb−Y·Se	31	79	109	130	259	272		39
Se_8 in Sr−Y·Se	30	75	107	122				30
monoclinic Se	50	84	114	128	249	254	239	46

[a] Frequencies in cm^{-1}.

tra of five different composites recorded at 647 nm[30,33,39] under vacuum. Photoinduced structural changes of the light-sensitive semiconductor can be easily avoided at this excitation energy (1.91 eV as compared with the band gaps in Table 3). The spectra have been normalized by the Bose−Einstein factor to remove their temperature dependence: $I = I_{obs}[1 - \exp(-h\nu/k_BT)]$, $T = 300$ K.[30,33−35,39] They consist of broad glasslike and narrow molecular Se bands separated into two groups: low-frequency torsional (≤50 cm^{-1}) and bending (50 ≤ ω ≤ 150 cm^{-1}) modes and high-frequency stretching modes (150 cm^{-1} ≤ ω ≤ 300 cm^{-1}).[42]

Disordered Chains. The predominant broad bands are similar to those observed in *a*-Se and liquid Se and can therefore be attributed to disordered Se chains.[30,31,34] The blue shift of the 262 cm^{-1} Se band and its 240 cm^{-1} shoulder in La−Y, Ca−Y, and Sr−Y relative to the corresponding bands in *a*-Se at 235 and 250 cm^{-1}, respectively, result from the loss of interchain bonding and concomitant strengthening of intrachain bonds in the confined Se chains. For the same reasons, the stretching bands in *a*-Se are blue-shifted with respect to the corresponding modes of *t*-Se helices at 233 and 237 cm^{-1}.[9] The additional shift of the confined Se bands confirms that the Se chains in zeolite Y are virtually isolated.[34] Note that Cu^{2+}−Se interactions soften these stretching modes in the Cu−Y composite, as evidenced by the red-shifted maximum at

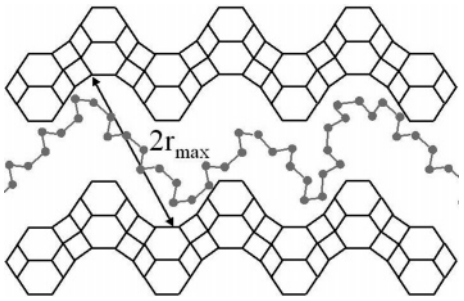

FIGURE 6. Schematic of the Se chain arrangement inside the faujasite pores.

241cm^{-1},[33] consistent with the optical spectrum and the short-range structure.

The most striking chain-related Raman feature in the low-frequency region is the strong scattering of the Ca−Y, Sr−Y, and La−Y composites below 60 cm^{-1} (Figure 5). Its absence in the spectra of Se in the Cu−Y and Rb−Y composites corroborates its link to the chain dynamics because chains are absent in Rb−Y, and in Cu−Y, their flexibility is considerably reduced due to the tight bonding of Se to Cu^{2+}. This low-frequency scattering is reminiscent of boson peaks[34,35] and can be rationalized in terms of localized phonons. Using the Ioffe−Regel condition, ($\omega \approx v_s/2r$),[43] where ω is the scattering frequency and v_s = 1050 m s^{-1}, the transverse sound velocity of *a*-Se, a mean localization length $2r = 15 \pm 4$ Å is estimated from the band maxima between 18 and 31 cm^{-1} in Ca−Y, Sr−Y, and La−Y.[34,35] This distance agrees well with the dimensions of the faujasite framework and corresponds to segments of 10 ± 3 atoms within the polymeric Se chains.[35] Chain segments located within the supercage windows probably prefer a helical configuration due to geometrical constraints, but the tetragonal symmetry of the faujasite pore system limits their length to less than two supercage diameters (i.e., ≤ 25 Å). To extend into a third cage, a chain has to bend at an angle (Figure 6), which could disrupt the synchronized movement of Se atoms along the chain and lead to localized collective librational or translational excitations at frequencies below 50 cm^{-1} as in fact are observed.

Se_8 Rings. The narrow Raman bands of the La−Y, Ca−Y, and Sr−Y composites are assigned to Se_8 rings based on ab initio quantum chemical calculations.[30,44,45] The agreement is surprisingly good (Table 3), indicating very weak interactions between rings and with the hosts. For comparison, the intermolecular interaction in *m*-Se crystals results in blue-shifted bending and red-shifted stretching Se_8 modes (Table 3).[46] The fraction of rings increases in the composites going from La−Y to Ca−Y and Sr−Y,[30] but they are completely absent in Cu−Y.[33] The predominant broad bands indicate that disordered Se chains dominate in these composites,[30] but they are virtually absent in the Rb−Y composite (Figure 5).[39] The bands of Se in Rb−Y can be divided into two groups based on their excitation energy dependence:[39] one set originates again from Se_8 rings (Table 3), while the second is attributed to stable Rb^+/Se_8 coordination complexes leading to lifted degeneracies (98 cm^{-1}), the appearance of librational (48

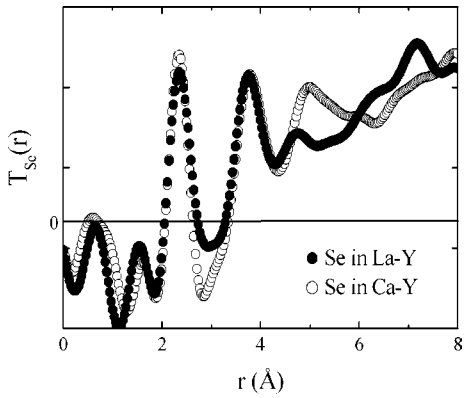

FIGURE 7. Difference pair distribution functions of Se confined in La−Y and Ca−Y zeolites.

and 64 cm^{-1}) and cation-related (136 cm^{-1}) modes, and red-shifted fundamental Se_8 modes (250 and 263 cm^{-1}).[39] Coordination complexes between neutral chalcogen clusters and alkali ions have not been directly observed before in molecular sieves. The exact nature of Rb^+/Se_8 coordination complexes in Rb−Y is unknown but could be similar to crown-ether-like and edge-on Rb^+-coordinated Se_8 rings in the crystalline polyselenide $Rb_2[Pd(Se_4)_2]\cdot Se_8$.[39,47] However, Rb^+ obviously exerts a pronounced structure-directing effect on Se in zeolite Y, prompting the complete cyclization of the chalcogen.

Stability. Strong interchain bonding is a key characteristic of bulk *t*-Se and *a*-Se, but Se chains are largely isolated inside zeolite pores, and intermolecular forces are reduced to a minimum. Many zeolites absorb Se without difficulty, indicating that host−guest interactions compensate sufficiently for the loss of interchain bonding. To evaluate the relevance of Se−cation interactions, we studied the competitive sorption of Se into Ca−Y and La−Y.[38] La^{3+} ions occupy only sodalite cages, whereas Ca^{2+} ions are also found in the supercages next to the encapsulated Se. Preloaded La−Y with 13.5 Se atoms per supercage and pure Ca−Y were filled into two arms of a quartz tube separated by a frit. After sealing both arms under vacuum, heating to 350 °C led within a few days to an almost complete transfer of the Se to the Ca−Y according to the net reaction[38]

$$0.9\text{La}-\text{Y}\cdot 13.5\text{Se} + \text{Ca}-\text{Y} \rightleftarrows 0.9\text{La}-\text{Y}\cdot 0.8\text{Se} + \text{Ca}-\text{Y}\cdot 11.5\text{Se} \quad (1)$$

The superior stability of the Ca−Y composite clearly demonstrates the existence of Ca^{2+}−Se interactions.[38] The length scale of this interaction was assessed by AXS measurements. Figure 7 shows the $T_{Se}(r)$ obtained from the Ca−Y and La−Y composites.[38] There is a remarkable overall agreement below 4 Å, where the first- and second-neighbor Se−Se interactions dominate, but differences appear around 5 Å. These additional Se-related correlations in Ca−Y can be attributed to Ca^{2+}−Se chain interactions[38] since the Raman spectra imply negligible interaction between the Se_8 rings and the hosts. Se-framework interactions (Se−Si, Se−Al, and Se−O) may be contributing to these new correlations since the flexible chains are drawn closer to the aluminosilicate walls through the interactions with the framework-coordinated cations. This precludes the determination of reliable Ca^{2+}−Se coordination numbers. Nevertheless, the long correlation length indicates very weak interactions as compared with the Cu^{2+}−Se charge-transfer interactions at 3.3 Å (Figure 4). It is also shorter than the 3.9 Å average Rb^+−Se distance in Rb^+−Se_8 coordination complexes in a crystalline polyselenide.[47]

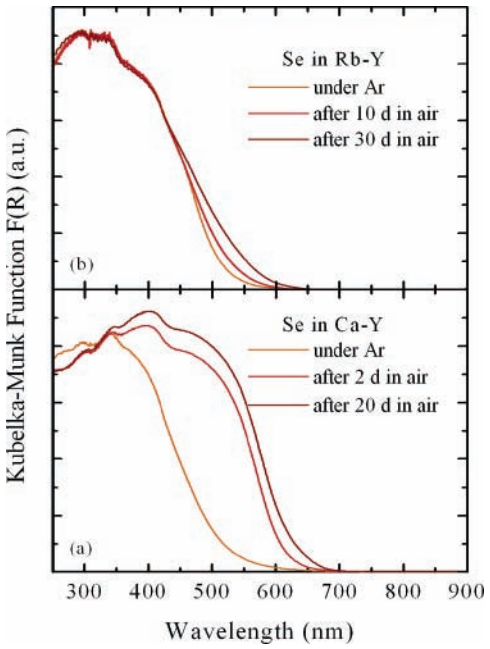

FIGURE 8. Optical behavior of Se in (a) Ca−Y and (b) Rb−Y zeolites as function of time in air.

The weak Ca^{2+}−Se interactions are not sufficient to stabilize the composite under ambient conditions. Upon exposure to air, the Ca−Y composite undergoes a rapid color change from bright orange to deep ruby-red, and within 2 days, the optical spectrum resembles that of *a*-Se (Figure 8a).[39] The deposition of *a*-Se on the zeolite surface is confirmed by Raman spectroscopy.[39] Since the Raman spectra do not indicate oxidized Se species, the release of Se chains from the pores is likely triggered by moisture. Water molecules could coordinate to Ca^{2+} ions and displace the Se chains from them. Deprived of the weak bond, the chains migrate to the surface and restabilize through interchain bonding.

Se rings are more bulky and therefore less mobile than chains within the faujasite pore system. Hence, the Se_8-containing Rb−Y composite is expected to be more stable under ambient conditions. This is confirmed by air-exposure experiments, which led only to minor changes of the optical and Raman spectra of the confined Se:[39] after 30 days, the main optical transitions were not affected, and slow changes at the absorption edge were attributed to traces of Se chains (Figure 8b).[39] The size of Se_8 is similar to the width of the supercage apertures, so that this ring is probably trapped even though water molecules are likely to interfere with their coordination to Rb^+ ions. Stable coordination of some rings to Rb^+ ions could also

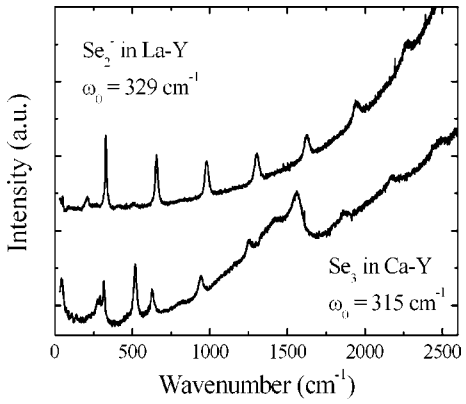

FIGURE 9. Resonance Raman spectra of Se photodecomposition products Se_2^- and Se_3 with characteristic hot fluorescence of Se_3 around 1500 cm^{-1}.

slow Se_8 diffusion within the pores and contribute to the stability of this composite in air.

Photochemistry.

Since selenium is a photosensitive semiconductor, the photochemical stability of confined Se is an obvious concern. Indeed, the Raman spectra of alkaline earth and rare earth exchanged composites change in a striking fashion when the excitation energy exceeds the band gaps.[36,37] Under irradiation with blue 476 nm laser light (=2.60 eV), the features originating from disordered Se chains gradually disappear, and new resonance Raman bands emerge along with strong fluorescence (Figure 9).[36,37] Analysis of the resonance spectra yields fundamental vibration frequencies ω_0 and anharmonicity constants $x_0\omega_0$, indicating the formation of neutral Se_3 (C_{2v}) clusters in Ca−Y (ω_0 = 315 cm^{-1}, $x_0\omega_0$ = 0.5 cm^{-1})[37] and Se_2^- radical anions in La−Y (ω_0 = 329 cm^{-1}, $x_0\omega_0$ = 0.8 cm^{-1})[37] and Nd−Y (ω_0 = 328 cm^{-1}, $x_0\omega_0$ = 0.7 cm^{-1}).[36] These assignments are corroborated by characteristic hot fluorescence bands for Se_3 in Ca−Y and Se_2^- in Nd−Y and by an additional band at 210 cm^{-1} in La−Y that originates from the excited $^2\Pi_u$ electronic state of Se_2^-.[36,37] Thus, photodecomposition products of the Se chains also depend on the counterions. Se_8 bands disappear together with the chain bands, but this is likely due to reactions with transient chain fragments. No photodecomposition products are observed after excitation of Se confined in Rb−Y zeolite at 476 nm,[39] confirming that Se_8 rings are more photostable.

The stabilization of chalcogen radical anions in aluminosilicates is not uncommon. Se_2^-, a chromophore of red ultramarine, forms at high temperatures (>900 °C) inside sodalite cages during crystallization of the aluminosilicate pigment.[48] In La−Y and Nd−Y, Se_2 probably forms in the supercages as chains break down under irradiation and then stabilizes through electron transfer from oxidic rare earth clusters inside the sodalite cages[36]

$$[La_2(OH)_2]^{4+} + Se_2 \leftrightarrows [La_2(OH)(O)]^{4+} + Se_2^- + H^+ \quad (2)$$

The formation of neutral Se_3 molecules in Ca−Y supports an active role of the rare earth clusters in the stabilization of Se_2^- in zeolite Y, although it is unclear whether it enters the sodalite cage there. Se_3 clusters are much less stable than larger ring clusters[44,49] and must therefore be stabilized in the Ca−Y composite. The bent C_{2v} ground state of Se_3 has singlet character corresponding to that of the homologous ozone O_3. The Se−Se bond distances indicate a bond order between one and two, pointing to a polarized mesomeric structure with a partial positive charge at the central and partial negative charges at the outer atoms.[44] Thus, Se_3 could make a strong bidental coordination to the exposed Ca^{2+} ions in type II sites. Neutral chain fragments or ring clusters other than Se_3 have not been observed after photodecomposition of Se chains in zeolite Y, except for small amounts of Se_6 rings in Ca−Y that probably form via dimerization of Se_3 clusters.[37]

Conclusion

Selenium/zeolite Y nanocomposites are readily obtained in a one-step process through sorption of the liquid or gaseous chalcogen at moderate temperatures, whereas the encapsulation of II−VI semiconductors in zeolites usually requires elaborate syntheses including reduction steps and the handling of poisonous gases such as H_2S and H_2Se.[50−52] We have shown that the host−guest interaction is a key factor in these nanocomposites, making it possible to tune their structural, electronic, and thermodynamic properties. The molecular character of Se can be shifted entirely from chains to rings through the interactions with the extraframework cations, leading to nanocomposites with enhanced optical and thermodynamic stability. While confinement broadens the band gap of Se, it can be reversed through interactions with transition metal ions in the zeolite hosts. The zeolite thus acts as a dopant, making it possible to shift the band gap below the bulk Se values. The principles governing selenium/zeolite composites apply to other materials where an arrangement between semiconductors and insulators is engineered. Examples include nanostructures of silicon,[53] germanium,[54] and II−VI semiconductors[50−52] confined in zeolites or other porous materials where the host can assume the role of a dopant. The host−guest interaction could also facilitate the confinement of elements such as bismuth,[55] which has so far presented challenges. While the investigation of the physicochemical aspects of host−guest compounds is still at an early stage, it is abundantly clear that the host−guest interaction represents one of the most intriguing facets of semiconducting nanocomposites.[56]

We thank our collaborators who have contributed their enthusiasm, ideas, and devoted efforts to these studies. Their names can be found in the papers cited herein. This work was jointly sponsored by the Office of Science of the U.S. Department of Energy, the SPM section of the Centre National de la Recherche Scientifique, and the Region-Centre. A.G. also acknowledges the Deutsche Forschungsgemeinschaft and the Fonds der Chemischen Industrie for research fellowships.

References

(1) Best, E.; Hinz, I.; Wendt, H. Selen. In *Gmelin Handbuch der Anorganischen Chemie*; Kugler, K. H., Ed.; Springer: Berlin, 1979; Vol. 10, pp 168−180.

(2) Alivisatos, A. P. Semiconductor Clusters, Nanocrystals, and Quantum Dots. *Science* **1996**, *271*, 933−937.

(3) Xu, R.; Husmann, A.; Rosenbaum, T. F.; Saboungi, M. L.; Enderby, J. E.; Littlewood, P. B. Large magnetoresistance in nonmagnetic silver chalcogenides. *Nature* **1997**, *390*, 57−60.

(4) Dimitrijevic, N. M.; Kamat, P. V. Photoelectrochemistry in Particulate Systems: 8. Photochemistry of Colloidal Selenium. *Langmuir* **1988**, *4*, 782−784.

(5) Abdelouas, A.; Gong, W. L.; Lutze, W.; Shelnutt, J. A.; Franco, R.; Moura, I. Using Cytochrome c_3 to Make Selenium Nanowires. *Chem. Mater.* **2000**, *12*, 1510−1512.

(6) Gates, B.; Yin, Y.; Xia, Y. A Solution-Phase Approach to the Synthesis of Uniform Nanowires of Crystalline Selenium with Lateral Dimensions in the Range of 10−30 nm. *J. Am. Chem. Soc.* **2000**, *122*, 12582−12583.

(7) Goldbach, A.; Johnson, J.; Meisel, D.; Curtiss, L. A.; Saboungi, M.-L. On the Constituents of Aqueous Polyselenide Electrolytes: A Combined Theoretical and Raman Spectroscopy Study. *J. Am. Chem. Soc.* **1999**, *121*, 4461−4467.

(8) Johnson, J. A.; Saboungi, M.-L.; Thiyagarajan, P.; Csensits, R.; Meisel, D. Selenium Nanoparticles: A Small-Angle Neutron Scattering Study. *J. Phys. Chem. B* **1999**, *103*, 59−63.

(9) Mott, N. F.; Davis, E. A. *Electronic Processes in Non-Crystalline Semiconductors*; Clarendon Press: Oxford, 1979.

(10) Breck, D. W. *Zeolite Molecular Sieves*; Wiley: New York, 1974.

(11) Sachtler, W. M. H. Metal clusters in zeolites: an intriguing class of catalysts. *Acc. Chem. Res.* **1993**, *26*, 383−387.

(12) Edwards, P. P.; Anderson, P. A.; Thomas, J. M. Dissolved Alkali Metals in Zeolites. *Acc. Chem. Res.* **1996**, *29*, 23−29.

(13) Ramamurthy, V.; Eaton, D. F.; Caspar, J. V. Photochemical and photophysical studies of organic molecules included within zeolites. *Acc. Chem. Res.* **1992**, *25*, 299−307.

(14) Bogomolov, V. N.; Lutsenko, E. L.; Petranovskii, V. P.; Kholodkevich, S. V. Absorption spectra of three-dimensionally ordered system of 12 Å particles. *JETP Lett.* **1976**, *23*, 482−484.

(15) Bogomolov, V. N.; Kholodkevich, S. V.; Romanov, S. G.; Agroskin, L. S. The absorption spectra of single selenium and tellurium chains in dielectric matrix channels. *Solid State Commun.* **1983**, *47*, 181−182.

(16) Bogomolov, V. N.; Poborchii, V. V.; Kholodkevich, S. V. Size effects in the vibrational spectrum of 10 Å selenium particles. *JETP Lett.* **1985**, *42*, 517−520.

(17) Terasaki, O.; Yamazaki, K.; Thomas, J. M.; Oshuna, T.; Watanabe, D.; Sanders, J. V.; Barry, J. C. Isolating individual chains of selenium by incorporation into the channels of a zeolite. *Nature* **1987**, *330*, 58−60.

(18) Parise, J. B.; MacDougall, J. E.; Herron, N.; Farlee, R.; Sleight, A. W.; Wang, Y.; Bein, T.; Moller, K.; Moroney, L. M. Characterization of Se-Loaded Molecular Sieves A, X, Y, AlPO-5, and Mordenite. *Inorg. Chem.* **1988**, *27*, 221−228.

(19) Endo, H.; Inui, M.; Yao, M.; Tamura, K.; Hoshino, H.; Katayama, Y.; Maruyama, K. Structure of Isolated Selenium Chain in the Channels of Mordenite. *Z. Phys. Chem. Neue Folge* **1988**, *156*, 507−511.

(20) Nozue, Y.; Kodaira, T.; Terasaki, O.; Yamazaki, K.; Goto, T.; Watanabe, D.; Thomas, J. M. Absorption spectra of selenium clusters and chains incorporated into zeolites. *J. Phys.: Condens. Matter* **1990**, *2*, 5209−5217.

(21) Poborchii, V. V.; Ivanova, M. S.; Petranovskii, V. P.; Barnakov, Yu. A.; Kasuya, A.; Nishina, Y. Raman and absorption spectra of zeolites A and X containing selenium and tellurium in nanopores. *Mater. Sci. Eng. A* **1996**, *217*−*218*, 129−134.

(22) He, L.; Shen, Z. X.; Gu, G.; Qin, L.; Tang, S. H. Luminescence due to the indirect band-gap transition activated by the inter-valence transition of Se clusters confined in 13X zeolite. *Chem. Phys. Lett.* **1999**, *300*, 504−508.

(23) Poborchii, V. V.; Lindner, G.-G.; Sato, M. Selenium dimers and linear chains in one-dimensional cancrinite nanochannels: Structure, dynamics, and optical properties. *J. Chem. Phys.* **2002**, *116*, 2609−2617.

(24) Simoncic, P.; Armbruster, T. Se incorporated into zeolite mordenite-Na: a single-crystal X-ray study. *Microporous Mesoporous Mater.* **2004**, *71*, 185−198.

(25) Tang, Z. K.; Loy, M. M. T.; Goto, T.; Chen, J.; Xu, R. Polarized Raman Spectra of Se Chains Isolated in Channels of $AlPO_4$-5 Single Crystal. *Solid State Commun.* **1997**, *101*, 333−336.

(26) Poborchii, V. V.; Kolobov, A. V.; Caro, J.; Zhuravlev, V. V.; Tanaka, K. Dynamics of Single Selenium Chains Confined in One-Dimensional Nanochannels of $AlPO_4$-5: Temperature Dependencies of the First- and Second-Order Raman Spectra. *Phys. Rev. Lett.* **1999**, *82*, 1955−1958.

(27) Wirnsberger, G.; Fritzer, H. P.; Zink, R.; Popitsch, A.; Pillep, B.; Behrens, P. Isolated Se_6 Rings in the Voids of a Weakly Interacting, Electroneutral, and Crystalline SiO_2 Matrix: Combined Experimental and Theoretical Study. *J. Phys. Chem. B* **1999**, *103*, 5797−5801.

(28) Demkov, A. A.; Sankey, O. F. Theory of zeolite supralattices: Se in zeolite Linde type A. *J. Phys.: Condens. Matter* **2001**, *13*, 10433−10457.

(29) Bichara, C.; Raty, J. Y.; Pellenq, R. J.-M. Adsorption of Selenium Wires in Silicalite-1 Zeolite: A First-Order Transition in a Microporous System. *Phys. Rev. Lett.* **2002**, *89*, 016101.

(30) Goldbach, A.; Iton, L.; Saboungi, M.-L. On the formation of isolated Se_8 rings in zeolites. *Chem. Phys. Lett.* **1997**, *281*, 69−73.

(31) Armand, P.; Goldbach, A.; Cramer, C.; Csencsits, R.; Iton, L. E.; Price, D. L.; Saboungi, M.-L. Seminconductors in the disordered state: From bulk to nanoscale. *J. Non-Cryst. Solids* **1996**, *205*−*207*, 797−802.

(32) Armand, P.; Saboungi, M.-L.; Price, D. L.; Iton, L.; Cramer, C.; Grimsditch, M. Nanoclusters in Zeolite. *Phys. Rev. Lett.* **1997**, *71*, 2061−2064.

(33) Goldbach, A.; Saboungi, M.-L.; Iton, L.; Price, D. L. Approach to band gap alignment in confined semiconductors. *J. Chem. Phys.* **2001**, *115*, 11254−1260.

(34) Goldbach, A.; Saboungi, M.-L. Optical Spectroscopy on Se_8 Clusters and Se Chains Embedded in Zeolite Matrices. *Ber. Bunsen-Ges. Phys. Chem.* **1997**, *101*, 1660−1664.

(35) Goldbach, A.; Saboungi, M.-L. Optical spectroscopy on Se clusters and chains confined in zeolites. *Eur. Phys. J. E* **2003**, *12*, 185−190.

(36) Goldbach, A.; Iton, L.; Grimsditch, M.; Saboungi, M.-L. The Formation of Se_2^-: A New Resonance Raman Feature in the Photochemistry of Zeolite-Encapsulated Selenium. *J. Am. Chem. Soc.* **1996**, *118*, 2004−2007.

(37) Goldbach, A.; Iton, L.; Grimsditch, M.; Saboungi, M.-L. Photoinduced Formation of Selenium Molecules in Zeolites: A Resonant Raman Spectroscopy Study. *J. Phys. Chem. B* **1997**, *101*, 330−334.

(38) Goldbach, A.; Saboungi, M.-L.; Iton, L.; Price, D. L. Stabilization of selenium in zeolites: an anomalous X-ray scattering study. *J. Chem. Soc., Chem. Commun.* **1999**, 997−998.

(39) Goldbach, A.; Iton, L.; Grimsditch, M.; Saboungi, M.-L. An air-stable selenium/zeolite nanocomposite. *Chem. Mater.* **2004**, *16*, 5107−5113.

(40) Raoux, D. Short- and medium-range order in noncrystalline materials by using anomalous scattering at large angles. In *Resonant Anomalous X-ray Scattering*; Materlik, G., Sparks, C. J., Fischer, K., Eds.; Elsevier Science B. V.: New York, 1994; pp 323−343.

(41) Price, D. L.; Saboungi, M.-L. Anomalous X-ray Scattering from Disordered Materials. In *Local Structure from Diffraction*; Billinge, S. J. L., Thorpe, M. F., Eds.; Plenum: New York, 1998; pp 23−33.

(42) Nakamura, K.; Ikawa, A. Medium-range order in amorphous selenium: Molecular dynamics simulations. *Phys. Rev. B* **2003**, *67*, 104203-1-12.

(43) Ioffe, A. F.; Regel, A. R. Non-Crystalline, Amorphous, and Liquid Electronic Semiconductors. In *Progress in Semiconductors 4*; Gibson, A. F., Kroger, F. A., Burgess, R. E., Eds.; Heywood: London, 1960; pp 237−291.

(44) Kohara, S.; Goldbach, A.; Koura, N.; Saboungi, M.-L.; Curtiss, L. A. Vibrational frequencies of small selenium molecules. *Chem. Phys. Lett.* **1998**, *287*, 282−288.

(45) The high-frequency Se_8 stretching modes are burried under the broad scattering bands of the disordered Se chains in La−Y, Ca−Y, and Sr−Y.

(46) Lucovsky, G.; Mooradian, A.; Taylor, W.; Wright, G. B.; Keezer, R. C. Identification of the Fundamental Vibrational Modes of Trigonal, α-Monoclinic, and Amorphous Selenium. *Solid State Commun.* **1967**, *5*, 113−117.

(47) Wachhold, M.; Kanatzidis, M. G. Powerful Templating Effect in Rb/Pd/Se_x Promoted by Crown Ether-Like $[Rb_2[Pd(Se_4)_2]\cdot Se_8$: A Layered Pd Polyselenide with Encapsulated Eight-Membered Selenium Rings. *J. Am. Chem. Soc.* **1999**, *121*, 4189−4195.

(48) Reinen, D.; Lindner, G.-G. The nature of the chalcogen color centres in ultramarine-type solids. *Chem. Soc. Rev.* **1999**, *28*, 75−84.

(49) Becker, J.; Rademann, K.; Hensel, F. Generation of Intense Selenium and Tellurium Cluster Beams. *Z. Phys. Chem.* **1991**, *173*, 21−24.
(50) Moller, K.; Eddy, M. M.; Stucky, G. D.; Herron, N.; Bein, T. Stabilization of Cadmium Selenide Molecular Clusters in Zeolite Y: EXAFS and X-ray Diffraction Studies. *J. Am. Chem. Soc.* **1989**, *111*, 2564−2571.
(51) Brigham, E. S.; Weisbecker, C. S.; Rudzinski, W. E.; Mallouk, T. E. Stabilization of Intrazeolitic Cadmium Telluride Nanoclusters by Ion Exchange. *Chem. Mater.* **1996**, *8*, 2121−2127.
(52) Brühwiler, D.; Leiggener, C.; Glaus, S.; Calzaferri, G. Luminescent Silver Sulfide Clusters. *J. Phys. Chem. B* **2002**, *106*, 3770−3777.
(53) He, J.; Ba, Y.; Ratcliffe, C. I.; Ripmeester, J. A.; Klug, D. D.; Tse, J. S.; Preston, K. F. Encapsulation of Silicon Nanoclusters in Zeolite Y. *J. Am. Chem. Soc.* **1998**, *120*, 10697−10705.
(54) Dag, Ö.; Kuperman, A.; Ozin, G. A. Germanium Nanoclusters: Chemical Vapor Deposition of Digermane in Zeolite Y and Mordenite. *Adv. Mater.* **1994**, *6*, 147−150.
(55) Benoit, R.; Saboungi, M.-L.; Treguer-Delapierre, M. Effect of radiation dose on the size of bismuth particles produced by radiolysis. *Eur. Phys. J. D* **2003**, *24*, 123−126.
(56) Nassimbeni, L. R. Physicochemical Aspects of Host−Guest Compounds. *Acc. Chem. Res.* **2003**, *36*, 631−637.

AR040282Y